Article

Systems Structural Biology Analysis of Ligand Effects ~~in~~on ERα Predicts Cellular Response to Environmental Estrogens and Anti-hormone Therapies

Jerome C. Nwachukwu[1]
Sathish Srinivasan[1]
Nelson E. Bruno[1]
Jason Nowak[1]
Nicholas J. Wright[1]
Filippo Minutolo[2]
Erumbi S. Rangarajan[1]
Tina Izard[1]
Xin-Qui Yao[3]
Barry J. Grant[3]
Douglas J. Kojetin[4]
Olivier Elemento[5]
John A. Katzenellenbogen[6]
Kendall W. Nettles[1, 7, *]
knettles@scripps.edu

[1]Department of Cancer Biology, The Scripps Research Institute, 130 Scripps Way, Jupiter, FL 33458, USA

[2]Dipartimento di Farmacia, Università di Pisa, Via Bonanno 33, 56126 Pisa, Italy

[3]Department of Computational Medicine and Bioinformatics, University of Michigan Medical School, Ann Arbor, MI 48109, USA

[4]Department of Molecular Therapeutics, The Scripps Research Institute, 130 Scripps Way, Jupiter, FL 33458, USA

[5]Department of Physiology and Biophysics, Institute for Computational Biomedicine, Weill Cornell Medical College, 1305 York Avenue, New York, NY 10021, USA

[6]Department of Chemistry, University of Illinois, 600 South Mathews Avenue, Urbana, IL 61801, USA

*Corresponding author

[7]Lead Contact

Published: December 29, 2016

Summary

Environmental estrogens and anti-hormone therapies for breast cancer have diverse tissue- and signaling-pathway-selective outcomes, but how estrogen receptor alpha (ERα) mediates this phenotypic diversity is poorly understood. We implemented a statistical approach to allow unbiased, parallel analyses of multiple crystal structures, and identified subtle perturbations of ERα structure by different synthetic and environmental estrogens. Many of these perturbations were in the sub-Å range, within the noise of the individual structures, but contributed significantly to the activities of synthetic and environmental estrogens. Combining structural perturbation data from many structures with quantitative cellular activity profiles of the ligands enabled identification of structural rules for ligand-specific allosteric signaling—predicting activity from structure. This approach provides a framework for understanding the diverse effects of environmental estrogens and for guiding iterative medicinal chemistry efforts to generate improved breast cancer therapies, an approach that can be applied to understanding other ligand-regulated allosteric signaling pathways.

Nwachukwu et al. demonstrate that the full dynamic range of allosteric signaling outcomes can derive from perturbations that are within the noise of the typical 2–3 Å crystal structure, but can be revealed by parallel analyses of many receptor-ligand complexes.

Introduction

The nuclear receptor (NR) superfamily of transcriptional factors represent one of the largest classes of therapeutic drug targets due to their roles as master regulators of development, endocrinology, and metabolism. Many NRs, such as

estrogen receptor alpha and beta (ERα and ERβ) respond to a hormonal and metabolic milieu that includes high-affinity natural ligands such as estradiol, and an ensemble of lower affinity ligands such as the environmental estrogens (EEs) that lead to diverse endocrine-disrupting phenotypes, including cancer, infertility, and developmental abnormalities. The Endocrine Society and the International Federation of Gynecology and Obstetrics recently issued scientific statements of concern that endocrine-disrupting chemicals (EDCs) are provoking a public health crisis. People are routinely exposed to EDCs found in shampoos, cosmetics, pesticides, plastics, diet, and many other sources (Di Renzo et al., 2015; Gore et al., 2015). The diversity of potential outcomes from a single receptor is exploited in NR-targeted drug discovery to obtain desired activity profiles. For example, the anti-hormone therapies for breast cancer, called selective estrogen receptor modulators (SERMs), display various on-target side effects on bone mineral density and uterine proliferation (Grese et al., 1997).

The molecular underpinnings of SERM activity seen with EEs and ER-targeted drugs derive from allosteric signaling similar to biased signaling with G-protein-coupled receptors, where ligand-binding controls recruitment of different possible signaling complexes to distal binding sites. In the classical ERα signaling pathway, estradiol binding induces ERα dimerization and DNA binding at estrogen response elements (EREs) (Kumar and Chambon, 1988; Schwabe et al., 1993) (Figures S1A and S1B). The ligand-bound ERα recruits coregulator complexes with assorted enzymatic activities that remodel nucleosomes and regulate the basal transcription apparatus (Lonard et al., 2007; Metivier et al., 2003; Shang and Brown, 2002). ERα contains the modular NR superfamily domains, designated A–F (Figures S1B and S1C). These include an intrinsically disordered N-terminal domain containing a coactivator-binding site called activation function-1 (AF1), a DNA-binding domain (DBD), and a C-terminal ligand-binding domain (LBD) that contains the activation function-2 (AF2) surface. Importantly, NRs act as scaffold proteins with ligands that control receptor-protein and receptor-DNA interactions through subtle changes in LBD structure that have remained largely elusive.

A barrier to understanding how the chemical structure of ligands is interpreted by the receptor is that changes in a single atom are often sufficient to drive widely divergent outcomes (Grese et al., 1997), suggesting that signal transduction occurs at a sub-Å resolution, within the noise of the typical NR crystal structure. To understand how ligands control receptor activity, we implemented a systems biology approach that we call ligand class analysis, where we examine the structure and function of closely related ligands in a chemical class or series defined by a specific molecular scaffold, allowing visualization of an ensemble of structural changes in the LBD (Bruning et al., 2010; Nettles et al., 2008; Nwachukwu et al., 2016; Srinivasan et al., 2013). This enabled us to identify ligand-specific structural perturbations that drive different signaling outcomes, but this approach was largely qualitative and relied on visual recognition of structural patterns. Therefore, an unbiased approach with the ability to analyze ligands with diverse scaffolds rather than closely related ones is required to study EEs.

Here, we developed a quantitative and unbiased approach to structural analyses that allowed us to determine chemical and structural rules for allosteric signaling. We solved the crystal structures of ERα LBD complexes with the EEs, coumestrol, 4,4-dichlorodiphenyltrichloroethane (DDT), and zearalenone, and identified subtle ligand-specific perturbations of LBD structure. Using a training set of 42 diverse synthetic ERα ligands, we quantified corresponding perturbations in as many crystal structures and identified structural features that significantly predicted ERα-mediated transcriptional activity and proliferative responses. We validated these structural features in an independent set of ten published EE/ERα LBD structures and found an interatomic perturbation that strongly predicted ERα LBD activity, and surprisingly predicted ERβ activity more powerfully.

Results

Structural Features of ERα Interaction with Coumestrol, DDT, and Zearalenone

The mycoestrogen zearalenone (Figure S1A) is found in grain crops worldwide and leads to profound reproductive abnormalities including infertility, miscarriage, and trans-generation effects, especially prevalent in pigs (Schoevers et al., 2012). Similarly, coumestrol ingested from clover feed prevents ovulation in mares (Ferreira-Dias et al., 2013). DDT was widely used as a pesticide and was banned for endocrine disruption that was decimating certain bird populations. Coumestrol showed full ERα agonist activity in profiling assays (Figures 1A–1C) and stabilized the full agonist-bound LBD conformation (Figures 2A, S2A, and S2B; Table S1). In contrast, DTT and zearalenone showed partial agonist activities (Figures 1A–1C) and different structural perturbations of the LBD compared with estradiol (Figures 2B–2D and S2C–S2F). When superposed with the estradiol-bound structure, zearalenone made a 3 Å contact with h11 Leu525 of the estradiol-bound structure, which induced a 1.1 Å shift in h11 (Figure 2B, red arrow), defining an inter-model distance where h11 shifted away from h3 and toward h11′ in the dimer partner. This in turn directed a contact between Leu525 and h12 Leu544, allowing the ligand to shift h12 indirectly.

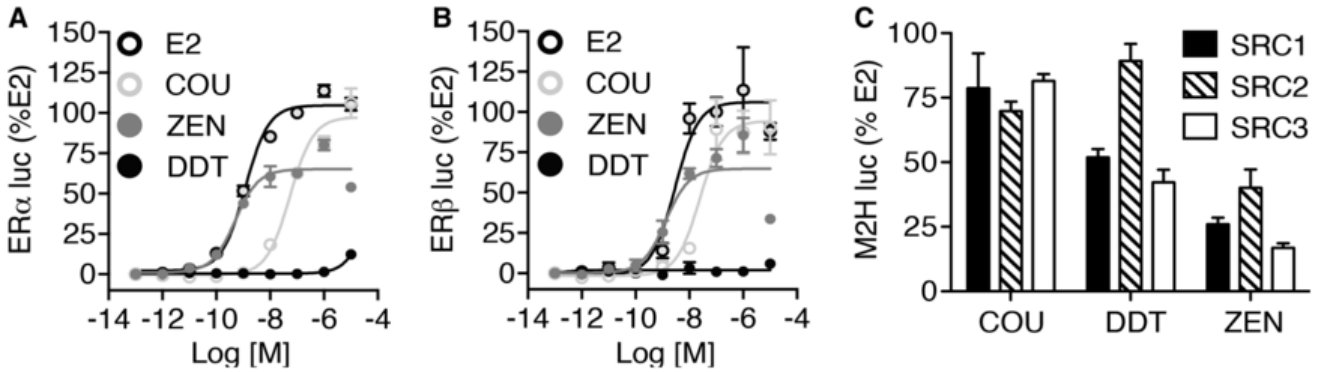

Figure 1 Biological Activity Profiles of Environmental Estrogens

(A and B) HepG2 cells were transfected with a 3xERE-driven luciferase reporter and ERα or ERβ expression plasmids and were treated with the indicated compounds for 24 hr. The mean ± SEM of triplicates are shown.

(C) ERα-VP16 interaction with Gal4-DBD fused to full-length SRC1/2/3 was compared with M2H assay in HEK293T cells stimulated with 10 μM of the indicated compounds for 24 hr. The means ± SEM of triplicates are shown. See also Figure S1.

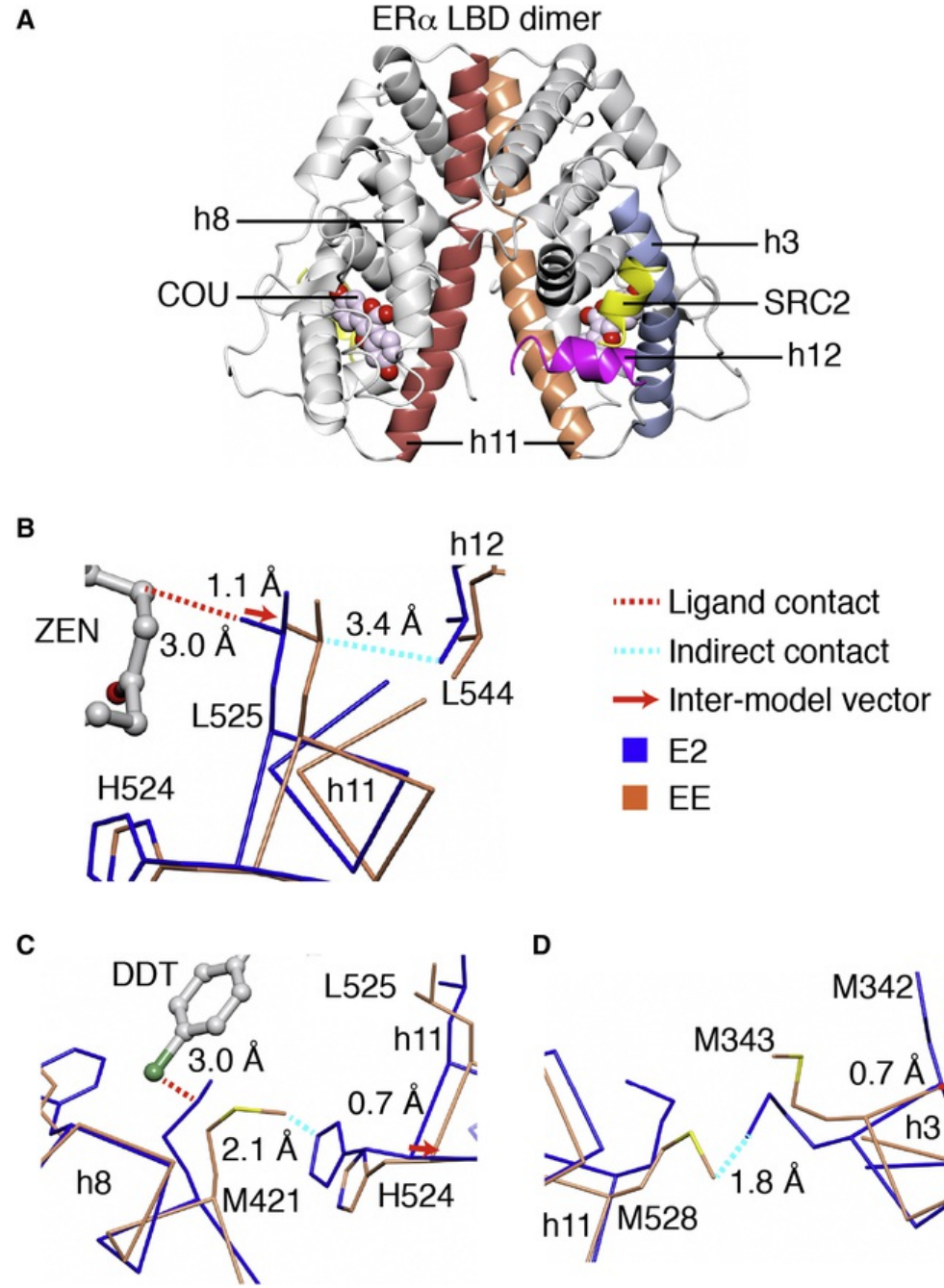

Figure 2 Effects of EEs on ERα LBD Structure

(A) Crystal structure of the coumestrol (COU)-bound LBD dimer in an active conformation where helix-12 (h12) docks across h11 and h3, with an SRC2 peptide docked at the AF2 surface. The ligand is shown as spheres.

(B) The zearalenone (ZEN)/ERα-LBD structure (coral) was superposed on the E2/ERα structure (PDB: 3UUD, blue), with the ligand shown as ball and stick.

(C and D) DDT/ERα superposed against the E2/ERα structure and colored as in (B), with the ligand shown as ball and stick. See also Figure S2.

DDT induced a distinct set of structural perturbations. One ring of DDT mimicked the A ring of estradiol, with the chlorine substituent in the same space as the A ring hydroxyl (Figures S2A and S2D). The slight tilt in this chlorophenyl ring was matched by a corresponding tilt in Phe404 to maintain a 90° edge-to-face interaction that is highly conserved in ERα crystal structures (not shown). The trichloromethyl group of DDT occupies the same space as the C ring and the C-18 methyl group of estradiol, and forms van der Waals contacts with h3 Thr347 and Ala350 (Figure S2D). When superposed with the estradiol-bound structure, h11 residues are too far away to contact the trichloromethyl group, but Leu525 shifts inward into the ligand-binding pocket to contact DDT (Figure S2D). The second ring of DDT docked against the base of h8 between Met421 and Phe425, and showed a 3 Å contact with Met421 of the superposed estradiol-bound structure (Figure 2C). In the DDT-bound structure, Met421 was shifted substantially, making a 2.1 Å close contact with the estradiol-positioned His524. This clash was resolved in the DDT structure by a 0.8 Å shift in h11 away from h8 and toward h12 (Figure 2C), which is orthogonal to the zearalenone-induced shift in h11. This shift in h11 explains the limited activity of DDT, and leads to a shift in h3 Met343 (Figure 2D) that is transmitted along h3 to the AF2 surface (Figure S2F), and we have previously shown that such shifts in h3 can alter coregulator recruitment preferences by changing the shape of the AF2 surface (Nwachukwu et al., 2014, 2016). Thus, DDT induced a shift in h3 that slightly modified the AF2 surface, and a shift in h11 that is perpendicular to that induced by zearalenone.

Identifying Intra-model Perturbation Distances for Predicting ER Activity

One of the major limitations of macromolecular structure determination as a means to understand ligand-specific signaling is that many perturbations observed in individual structures, including the 0.8–1.1 Å perturbations observed here for our new EE structures, are near the limits of detection for typical 2–3 Å NR structures (Figures 2B–2D). Traditionally, the only way to improve the reliability of observations would be to obtain higher-resolution structures, but this strategy does not connect individual perturbations to specific signaling outcomes. Therefore, to make this connection, we implemented a statistical approach to structural analysis by using perturbations visualized in the DDT- and zearalenone-bound ERα structures to compare multiple LBD structures with experimentally determined signaling outcomes. There are limitations to using the individual inter-model distances to make conclusions about ligand activity, as they are variable depending on the reference structure and method of superposing. We identified a series on intra-model distance vectors designed to capture the perturbations we visualized from the EE structures (Figures 3A–3E). The locations of the amino acids that define these distance vectors are shown in Figures 3A–3B. Based on the zearalenone-bound structure, which shifted h11 toward the dimer interface, we measured the h11 Leu525-Leu525′ and Ser527-Ser527′ α carbon distances across the dimer interface (Figure 3C). Based on the DDT structure, we identified other distance vectors including Thr347-Leu525 (Figure 3D), which measures h3 and h11 perturbations along the same axis as the Leu525-Leu525′ distance, and the orthogonal distance from h11 His524 to h8 Ile424 (Figure 3E). We also measured the Leu354-Leu525 and Leu347-Ser512 distances (Figures 3D and 3E), the latter representing a distance vector designed to be primarily sensitive to h3 perturbations, since Ser512 is not a pocket residue and does not show obvious ligand-induced shifts.

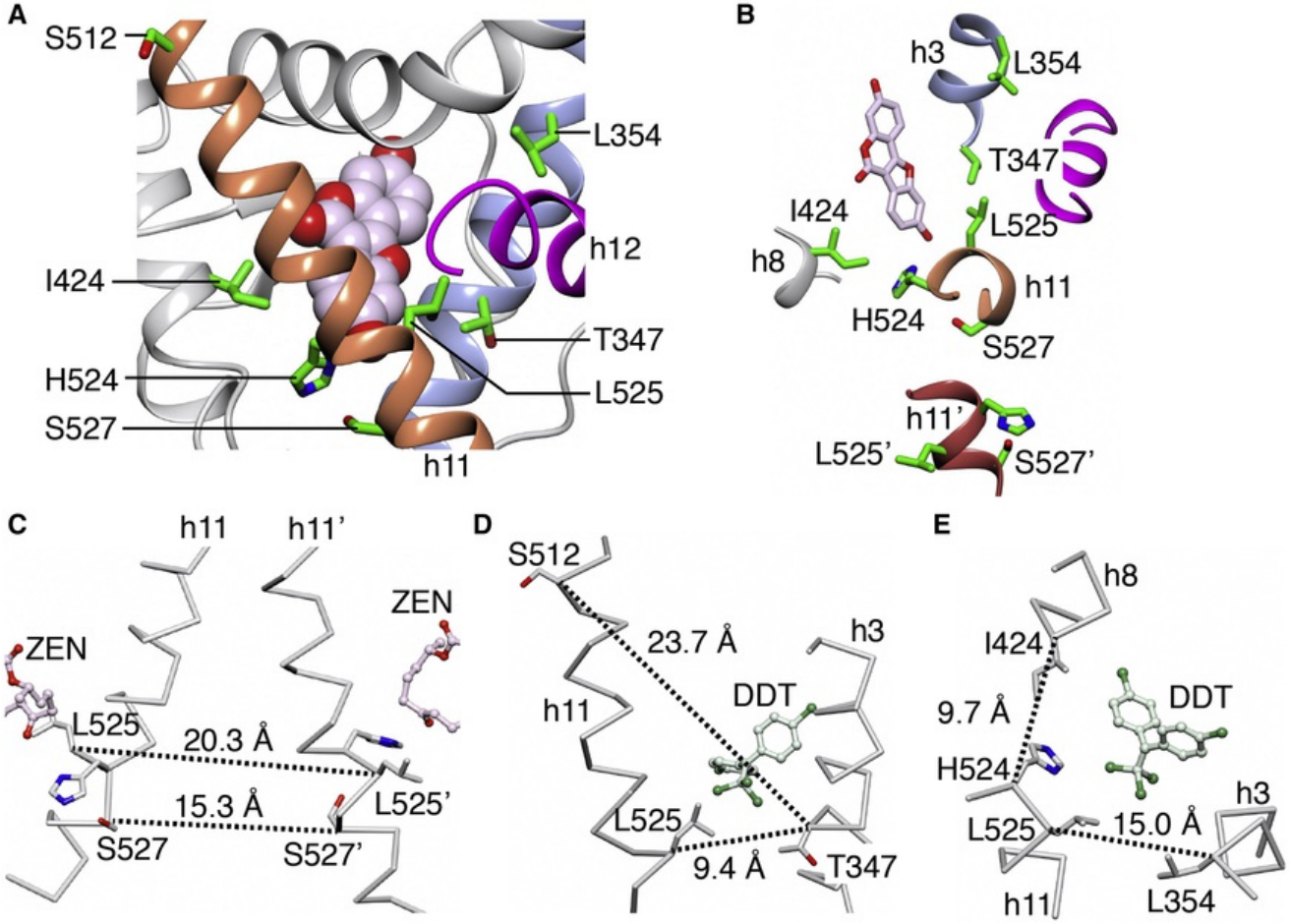

Figure 3 Intra-Model Distances for Ligand-Induced Perturbation of the ERα LBD

(A and B) Crystal structure of the COU-bound ERα LBD with positions of amino acid residues that define the set of intra-model distances colored green. The ligand is shown as spheres.

(C–E) Indicated helices from the crystal structures of the ZEN- or DDT-bound ERα LBD are shown as α carbon traces, with side chains shown as cylinders. Intra-model distances are shown as dashed lines. See also Figure S2.

From a set of 142 structures, we selected 42 LBD structures bound to diverse ligands (Table S2) that had completed profiling across 18 ER phenotyping assays (see Experimental Procedures; Figures S4A–S4D). We measured the intra-model distances in this 42-structure set and found SDs of 0.2–0.6 Å (Figure 4A). We also measured a set of six randomly selected distances, which displayed much less variance (Figures S3A and S3B). To assess the statistical significance of perturbations induced by individual ligands, we assigned error bars to the measurements. The diffraction-component precision index (DPI) estimates the error or SD(σ), in the position of each atom based on the number of reflections, resolution, B factors, and completeness of the data (Cruickshank, 1999; Kumar et al., 2015). The error in both atoms that define the distance measurement was added as described in Figure 4B and the Experimental Procedures. This allowed us to calculate whether each perturbation was statistically significant by assessing if it was greater than the 2σ significance threshold, corresponding to $p < 0.05$ for normally distributed data (Figure 4C). We calculated perturbations as deviations from either the mean distance or the corresponding distance in the 1.6 Å structure of the estradiol-bound LBD (PDB: 3UUD), and determined whether the ligand-specific deviations were greater than 2σ for each observation (Figure 4D). The source data and calculations can be found in Data S1. Only 30% of the observations made from these six distances in 42 structures were individually significant, and none of the Leu354-Leu525 perturbations exceeded the 2σ significance threshold (Figure 4D). Thus most of the structural perturbations measured were within the noise of the individual structure.

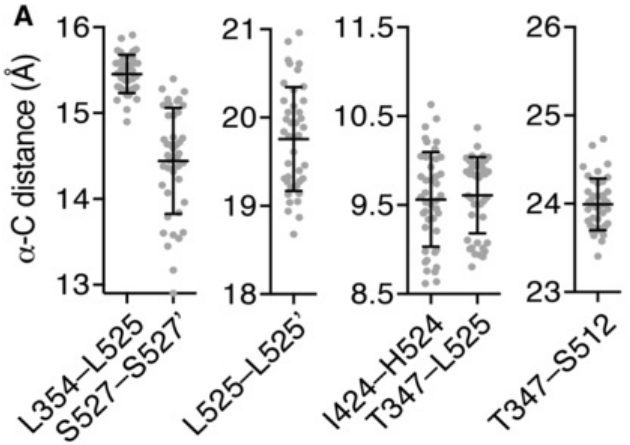

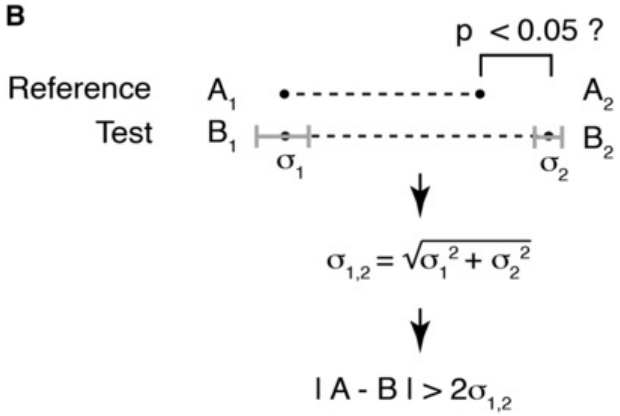

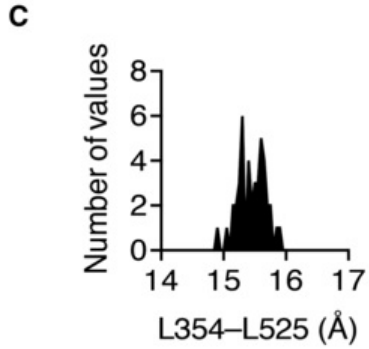

D

Distance (n = 42)	Significantly different from: mean	E2/ERα	%
L354–L525	0	0	0
S527–S527'	1	21	52
L525–L525'	3	16	45
I424–H524	5	12	40
T347–L525	2	9	26
T347–S512	1	2	7

Figure 4 Structural Perturbation in a 42-Structure Set

(A) The indicated α carbon distances were measured in the 42 crystal structures of the ERα LBD bound to different ligands, with lines showing the mean ± SD.

(B) Statistical test for determining significance of an interatomic difference measurement compared with a reference structural model.

(C) Frequency distribution for the L354-L525 distance measurements.

(D) Number of distances (n = 42) from (A) that exceed the 2σ significance threshold (or noise level) for LBD perturbations in individual structures. The source data and calculations can be found in Data S1 and further described in the Experimental Procedures section. See also Figure S3.

Predicting ER Activity in a Diverse Set of Synthetic Estrogens

We next tested whether the intra-model distances could predict estrogenic activity in our 42-ligand set. We have developed a quantitative and statistically robust high-throughput screening platform for ER phenotyping (Nwachukwu et al., 2016; Srinivasan et al., 2013). We measured canonical ERα-mediated phenotypes (Figures S4A–S4D), such as proliferation of MCF-7 breast cancer cells, with a counter-screen against proliferation of ERα-negative MDA-MB231 breast cancer cells, mRNA levels of the proliferative genes *GREB1* and *MYC*, and modulation of tumor necrosis factor alpha (TNF-α)-induced secretion of the inflammatory cytokine, interleukin-6 (IL-6), in MCF-7 cells. In addition, we measured ERα-DNA/protein interactions including dimerization, DNA binding, and mammalian 2-hybrid (M2H) interaction with full-length SRC1/2/3 transcriptional coactivator proteins that determine MCF-7 cell proliferation in a ligand-specific manner (Nwachukwu et al., 2016; Srinivasan et al., 2013). We also adapted the classic 3xERE-driven luciferase reporter transactivation assay to measure endogenous receptor activity in MCF-7 and Ishikawa cells, and the activities of wild-type (WT) and mutated receptors transiently expressed in HeLa, HepG2, and U2OS cells, cell lines that show significant differences in activity derived from AF1 (Figure S4C). Control curves for each of these assays have been published (Nwachukwu et al., 2016; Srinivasan et al., 2013). By examining compounds that had been screened in all of these assays, we identified 42 compounds that had also been visualized in crystal structures of the active ERα-Y537S LBD. These compounds derive from ten different scaffolds (Table S2) and demonstrated a wide range of estrogenic activities on the screening platform (Figures S4A–S4D), indicating structural and functional diversity. Importantly, none of the compounds significantly inhibited ER-negative MB-MDA231 breast cancer cell proliferation (Figure S4E); the source data can be found in Data S1.

To quantitate the predictive capacities of the structural distances (Figure 4A), we calculated Pearson's correlation coefficient, r, for pairwise comparisons with activity profiles, while the significance of these correlations was determined by p values calculated using the F test for non-zero slope (Table S3). After applying the Bonferroni correction for multiple hypothesis testing, three of the interatomic distances, Leu354-Leu525, Leu525-Leu525′, and I424-H524 correlated significantly with MCF-7 cell proliferation (Table S3

and Figure 5A). All three distances measure h11 perturbations and were highly inter-correlated (Table S3). The Thr347-Leu525 distance, which integrates h3 and h11 perturbations, also showed a trend toward significant correlation with proliferation. However, the interatomic distances showed weaker correlations with the expression levels of *GREB1* and *MYC* mRNA and secretion of IL-6 protein.

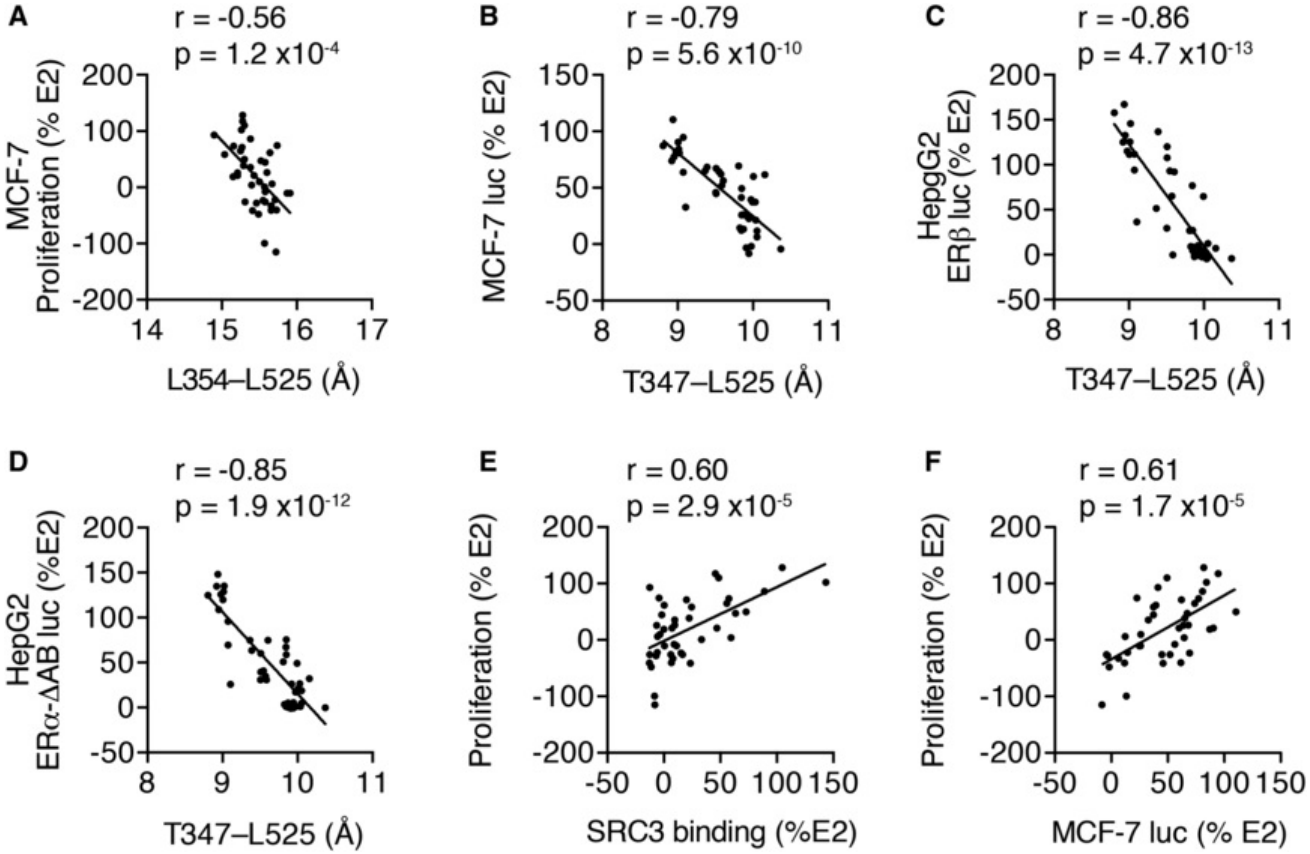

Figure 5 Prediction of ERα Activity in the 42-Ligand Set

The 42 ligands described in Table S2 were assayed at 10 μM doses for proliferation in MCF-7 cell or the indicated luciferase reporter (3xERE-luc), or mammalian-2-hybrid assays for interaction of ERα with SRC3, described further in Figure S4 and Experimental Procedures.

(A–D) Correlation analysis describing interatomic distance vectors calculated for each ligand-bound ERα LBD structure as predictors of ER activities. The Pearson's correlation coefficient, r, and the p value from the F test for non-zero slope are indicated.

(E and F) Correlation analysis showing signaling predictors of MCF-7 cell proliferation. See also Figures S4 and S5 and Tables S3, S4, and S5.

To understand the signaling features underlying these phenotypes, we asked whether these interatomic distances also predicted ligand-induced ERα-protein and ERα-DNA interactions. None of the distances predicted dimerization or DNA binding. Interatomic distances designed to measure both h3 and h11 perturbations showed different patterns of correlation with proliferation and ERα interaction with SRC1/2/3. Specifically, the Leu354-L525 distance significantly predicted proliferation but not SRC1/2/3 binding, while the Thr347-Leu525 distance did significantly predict SRC1/2/3 binding (Table S3). In contrast, the Ile424-His524 distance, which measures shifts between h8 and h11, and the L525-L525′ distance which measures h11 shifts toward the dimer interface significantly predicted both proliferation and SRC1/2/3 binding (Table S3). Thus, ligands can perturb different LBD sites to control recruitment of coactivators versus proliferation, reflecting diverse LBD-coregulator interactions that determine the ERα-mediated proliferative response, and functions of SRC1/2/3 interactions outside of proliferative phenotypes (Dasgupta et al., 2014).

Luciferase reporter assays provide us with an opportunity to test the structural prediction of ERα activity in the context of different cell types, and the impact of the AF1 coactivator-binding site on these relationships. This is important because SERMs such as tamoxifen are uterotrophic specifically through AF1 activity (McInerney and Katzenellenbogen, 1996), and we have recently shown that AF1 determines cell-type specificity in a ligand-specific manner (Nwachukwu et al., 2016). In tamoxifen-treated U2OS osteosarcoma and HepG2 liver cells, AF1 drives up to ~50% 3xERE-driven reporter activity relative to estradiol (Figure S4F). Tamoxifen acts via endogenous ERα in Ishikawa cells to produce ~10% reporter activity relative to estradiol, but has inverse agonist activity in MCF-7 and HeLa cells (Figure S4F). The interatomic distances generally correlated with reporter activity of WT ERα in cells with low tamoxifen-induced AF1 activity, including MCF-7 and HeLa cells, and ERβ activity in HepG2 cells (Table S3; Figures 5B and 5C), suggesting that AF1 interferes with the predictive power of these distance measurements.

To test this hypothesis, we examined correlations with the activity of ERα-ΔAB, which lacks AF1. Deletion of AF1 did not change the correlations with 3xERE-driven reporter activity in HeLa cells, but improved correlations with reporter activity in HepG2 and U2OS cells (Table S3), which is consistent with our hypothesis and the modulatory role of AF1 in ERα signaling. More importantly, it is striking that a single intra-molecular distance, Thr347-Leu525, was sufficient to predict 72% of the variation in ERα-ΔAB activity in HepG2 cells (Figure 5D, $r = -0.85$, $r^2 = 0.72$), and over 60% of the variation in endogenous ERα activity in MCF-7 cells ($r = -0.79$, $r^2 = 0.62$). Surprisingly, ERβ activity in HepG2 cells was much better predicted than full-length ERα activity (Table S3), consistent with the fact that AF1 of ERα is generally more transcriptionally active than that of ERβ (McInerney et al., 1998). We also tested deletion of the C-terminal F domain, which had the opposite effect, or less-significant correlations compared with deleting the AB domain (Table S3). One exception was the S527-S527′ distance, which gained significance in predicting the activity of ERα-ΔF. Thus, the ligand-LBD receptor interface initiates signals that are modulated by the AB and F domains to determine signaling specificity.

Molecular Predictors of ERα-Mediated Proliferation

We used a cross-correlation matrix to identify predictors of *MYC* and *GREB1* expression, IL-6 secretion, and MCF-7 cell proliferation in response to the 42 diverse compounds in the training set (Table S4). 3xERE-driven ERα activity in HepG2 cells correlated with *GREB1* expression. In contrast, *MYC* expression and IL-6 secretion did not correlate with any of the other activity profiles. Proliferation was predicted by SRC1/2/3 binding (Figure 5E), as well as the AF2-driven luciferase assays (Figure 5F). However, it was surprising that ERα interactions with SRC1/2/3 were generally weak predictors of expression of these target genes. While IL-6 has been shown to be a driver of oncogenesis (Rokavec et al., 2012), its modulation by ERα ligands did not predict proliferation (Table S4).

Given the number of highly significant predictors, we assessed whether combining them would improve the predictive power. We used multiple linear regression and systematically added independent variables to the regression equation. To evaluate these models, we calculated the coefficient of multiple correlation, R^2, a fraction that ranges from 0 to 1 and represents the percentage of the proliferative response that can be predicted by a given model. We used the F statistic to assess the impact of multiple hypothesis testing on the dependent variable, proliferation. The Leu354-Leu525 distance was selected as the most significant structural predictor of proliferation (Table S4). SRC1/2/3 binding were highly co-linear variables, with r ranging from 0.85 to 0.94 for the pairwise correlations between these interactions; therefore we used SRC3 binding as an independent variable. We also tested DNA binding, *GREB1* expression, and 3xERE-driven activity in MCF-7 cells as independent variables. The combination of Leu354-Leu525 and SRC3 binding produced an R = 0.70, with an adjusted $R^2 = 0.46$ ($F = 17.37$, $p = 4.8 \times 10^{-6}$, Table S5). Addition of the DNA binding, *GREB1*, or 3xERE-driven activity in MCF-7 cells as independent variables produced marginally higher adjusted R^2 values, but these variables did not contribute significantly to the model. While we decided a priori to calculate the average distance from both subunits of the dimer, there were some modest differences between the chains, and using only the Leu354-Leu525 distance in the B chain and SRC3 binding produced an R = 0.73, with an adjusted $R^2 = 0.51$ for predicting proliferation, demonstrating that slight differences in crystal packing may impact the predictive capacity of interatomic distances. Thus we were able to significantly predict the ligand-specific proliferative response from a single interatomic distance vector and M2H interaction between ERα and SRC3.

Given that most of the perturbations were within the noise of the individual structures, we wondered whether there was an effect of crystal resolution. We tested whether the distance measurements were predicted by resolution, but the r^2 values for each distance with respect to resolution was <0.02 showing no relationship (Figure S5A). We also binned the 42 structures into higher- and lower-resolution groups and found no significant differences in predictive power between the two groups (Figures S5B and S5C). As another control we tested the predictive power of the six randomly chosen distances (Figures S3A and S3B), and they did not significantly predict any of the bioassays after Bonferroni correction of the p value significance threshold for the correlation matrix. Lastly, we wanted to know if our longstanding use of a surface point mutation, Y537S, to facilitate crystallization impacted the distances. We and others have shown that this mutation stabilizes the active conformer without altering ligand binding (Delfosse et al., 2014; Nwachukwu et al., 2013, 2016), which allows us to soak pre-formed crystals and crystallization of ligands that would render the WT receptor conformationally heterogeneous. Comparing WT and Y537S structures bound with the same three ligands, the six distance measurements showed a remarkable similarity ($r = 0.998$, $p = 1.3 \times 10^{-20}$) (Figure S5D), demonstrating that the WT LBD, which has proven difficult to crystallize to due conformational heterogeneity, is unlikely to yield better predictors than the Y537S LBD.

Cross-Validation Studies Predicting ER Activity in a Set of EEs

To validate the predictive capacity of the six structural distances as determinants of estrogenic activity, we tested our statistical approach on an independent dataset. For this test, we took advantage of structure-activity data on 11 EEs, including estradiol using previously published crystal structures and activity data (Figures S6A and S6B), which also used the Y537S mutant to enable crystallization (Delfosse et al., 2014). In this smaller test set, the Ser527-Ser527′ distance predicted the activities of all four WT and AF1 deletion mutant receptors (Figure 6A), while both Leu525-Leu525′ and Ser527-Ser527′ significantly predicted ERβ-ΔAB luciferase activity after Bonferroni correction (Table S6). In contrast, the Ile424-His524 and Thr347-Ser512 distances were not predictive in this dataset. By computing the r^2 of these correlations, we found that the best predictor, Ser527-Ser527′, had predictive powers ranging from 41% to 75% across the four activity profiles. As a control, we re-refined the structures using simulated annealing to remove molecular replacement bias and found that the distance measurements were essentially identical (Figure S6C), with no effect on the correlation analyses.

A

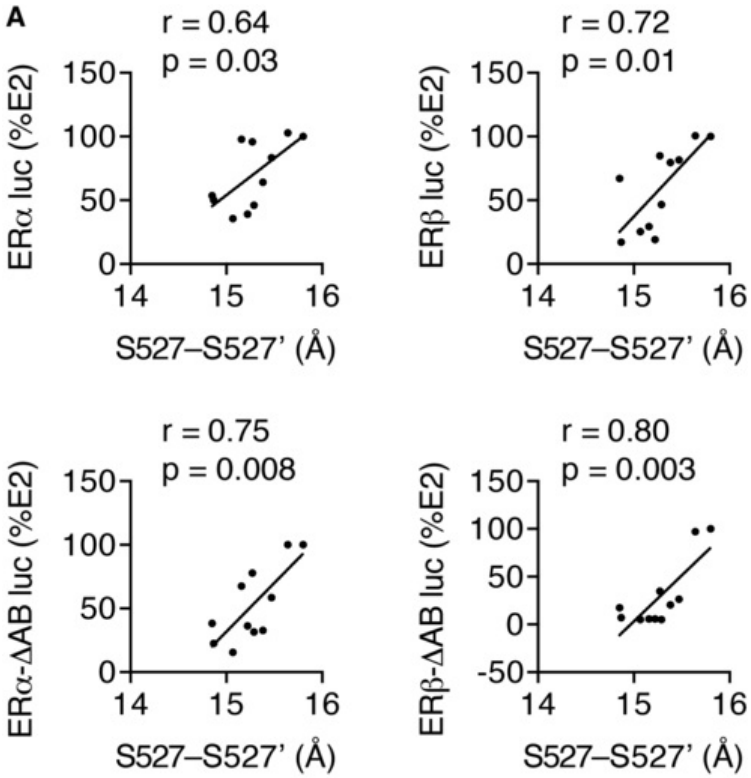

B

Distance (n = 11)	Significantly different from: mean	E2/ERα	%
L354–L525	0	0	0
S527–S527'	0	1	9
L525–L525'	1	3	36
I424–H524	2	3	45
T347–L525	0	1	9
T347–S512	0	1	9

Figure 6 Prediction of ERα and ERβ Activity in an Independent Test Set of EEs

(A) Correlation analysis of Ser527-Ser527′ α carbon distances and previously published activity profiles. HeLa cells stably expressing ERE-Luc and either ERα or ERβ, or constructs lacking the N-terminal AB domain, were generated according to Delfosse et al. (2014). Pearson's correlation coefficient, r, and the p value from the F test for non-zero slope are indicated.

(B) Number of distances (n = 11) from (A) that exceed the $2\sigma_{1,2}$ significance threshold (or noise level) for LBD perturbations in individual structures. The source data and calculations can be found in Data S1 and are described in the Experimental Procedures. See also Figure S6 and Table S6.

For each distance in the EE-bound structures, we again calculated deviations from the mean distance or the distance observed in the estradiol-bound reference structure (Figure 6A, Data S1), and found once again that most of the ligand-induced perturbations along the distance vectors were within the statistical noise of the individual structures. This demonstrates that our statistical approach enables the use of super-resolution data to predict receptor activity from crystal structures, and that the full range of biological activity can be driven by subtle ligand-directed perturbation of the LBD.

Validation of Distance Measurements in a 142-Structure Set

As another validation approach, we asked to what extent the perturbations identified in our 42-ligand set, described in Tables S1 and S2, are relevant to our full structural dataset of 142 ligands (Data S2). Hierarchical clustering of the distance measurements in the larger structure set revealed three main clusters (Figure 7A). We then used principal component analysis to identify the uncorrelated major components of h11 variance. Principal components 1 and 2 (PC1 and PC2), which capture the most variance in h11 position, were plotted for each structure and colored based on the hierarchical clustering (Figure 7B). This revealed that the selected distance measurements captured the major sources of variance around h11. PC1 consisted of a movement of the C terminus of h11 toward and away from the dimer interface (Figure 7C). In contrast, PC2 showed the C-terminal of h11 in one monomer and the N-terminal of the other h11 suggesting a twisting movement in the z-plane of the image (Figure 7C).

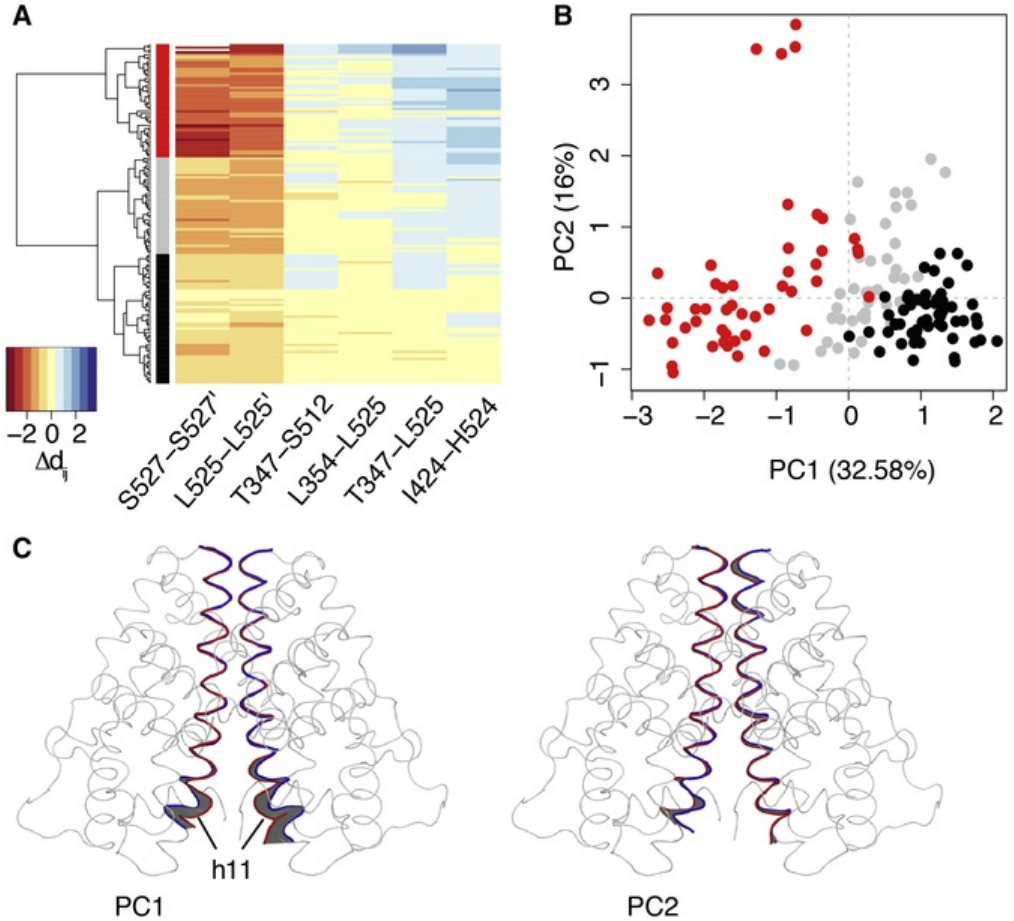

Figure 7 Select Atomic Distances Reveal Clusters of Structures That Are Consistent with Principal Component Analysis Results

(A) Clustering of 142 structures of the ERα LBD based on the six atomic distances. Each row of the matrix on the right represents a structure and each column represents a particular atomic distance. The matrix is color coded by the difference distance between each structure and the reference estradiol-bound structure (PDB: 3UUD). The left dendrogram is resulted from a hierarchical clustering using the six characteristic difference distances as the metric of dissimilarity (see Experimental Procedures for more details). Three clusters are indicated with red, gray, and black blocks.

(B) Projection of structures (round points) onto the PC1-PC2 subspace derived from a principal component analysis focused on H11 (see Experimental Procedures for more details). The color scheme of points is the same as that colors clusters in (A).

(C) Collective structural change of H11 revealed by PC1 and PC2. Red and blue tubes represent the minus and plus ends, respectively, of the structural change along PCs. Gray shaded areas between tubes indicate the trajectory of structural change. Other parts of protein are colored white. See also Data S2.

Discussion

In this work we implemented a systems biology approach to decipher how ER ligands control gene expression and proliferation of breast cancer cells. Structures of the ERα LBD bound to the EEs coumestrol, zearalenone, and DDT revealed different conformational perturbations that impact receptor activity in unpredictable ways. To identify structural rules for ERα-mediated activities, we defined intra-model distance vectors for ligand-induced shifts in h3 and h11. We tested the predictive capacity of these vectors on a set of 42 synthetic ligands bearing ten different scaffolds, and on an independent set of previously published structure-activity data for 11 EEs, including estradiol. We previously established that predictive rules for ERα activity could be derived for certain closely related ligands with the same scaffold and thus perturb the receptor similarly (Nwachukwu et al., 2016; Srinivasan et al., 2013). This work demonstrates that predictive models can also be developed for ligands with diverse scaffolds by using X-ray crystallography as a systems biology tool, instead of visualizing and comparing individual structures. Combining structural and molecular variables using multiple regression analysis allowed us to identify predictors of proliferation and reporter gene activity. The predictive capacity of structural variables was cross-validated in a published set of EEs, demonstrating the possibility of identifying statistical predictors of endocrine disruption based on

crystal structures and a few quantitative bioassays.

The use of intra-model distance vectors for statistical analyses of multiple structures represents an advance toward utilizing X-ray crystallography as a systems biology technique. The variance for some of these vectors is very small, and cannot be visualized in an individual structure. This approach is analogous to the use of sampling of photons from multiple point sources in super-resolution microscopy to generate a statistical distribution that defines location more precisely than a diffraction-limited conventional image (Thompson et al., 2012). However, in this case we are not obtaining super-resolution information about an individual structure, but rather from the analysis of many structures in parallel. For this reason, we have called this approach super-resolution structural analysis, rather than super-resolution X-ray crystallography, to indicate differences in the analogy. For the dataset published by Delfosse et al. (2014), the full dynamic range of activities was predicted from 0.25 to 0.5 Å shifts in h11, which is within the noise of the typical NR LBD structure. The direction of ligand-induced perturbation is not necessarily the same as the distance vector that predicts activity, thus it is still unclear how a ligand-specific structural perturbation is resolved to control multiple signaling pathways. Identifying orthogonal distance vectors that predict different signaling outcomes will enable the rational design of ligands with pathway- or tissue-selective activity profiles.

It is remarkable that a single interatomic distance vector in the ERα LBD predicted over 70% of some ERα and ERβ activities, while the combination of a distance vector and SRC3 binding profiles predicted ~50% of the proliferative response in MCF-7 breast cancer cells. Also, we previously identified the OBHS-N ligand series where >90% of the proliferative response could be predicted from a single biochemical variable such as SRC3 binding or *GREB1* expression (Nwachukwu et al., 2016). Our work suggests that the same level of success could be achieved for diverse EEs or other heterogeneous ligands by identifying the most important molecular and structural determinants of ER-mediated tissue-selective and developmental outcomes.

We previously identified shifts in h11 as the mechanism for partial agonist activity, noting that in the active LBD conformation, the positioning of h11 controls the docking of h12 (Nettles et al., 2008). However, this work demonstrates that the h11-sensitive distance vectors have important signaling consequences. Some h11 perturbations also shift the static position of h12, changing the shape of the AF-2 surface. This and other recent work demonstrates that ligands can perturb the AF2 surface more directly through h3 (Nwachukwu et al., 2014, 2016). Thus, we are beginning to decipher how different ligands can affect both the percentage of time AF2 is active via h11-mediated control of h12 dynamics versus controlling the shape of the AF2 surface by distorting h12 and h3. We still do not understand how ligands in the LBD control activity of other domains such as DNA binding, AF1 activity, or the role of the F domain in inter-domain communication and control of SERM agonist activity (Montano et al., 1995; Patel and Skafar, 2015). It was surprising that crystal structures of the ERα LBD are better predictors of ERβ activity compared with ERα. We attribute this to the relatively weak contribution of AF1 to ERβ activity in the 3xERE-driven reporter assay (McInerney et al., 1998), given that the ligand-binding pockets of ERα and ERβ are structurally similar with only two different amino acid residues. Consistent with this idea, ERα activity was more predictable without AF1 as observed with the ERα-ΔAB construct.

Current limitations of our approach are due to the lack of in vivo datasets on which structural and biochemical predictors can be trained or cross-validated, and an incomplete understanding of the ensemble of ligand-selective target genes and coregulators that govern cell proliferation and/or differentiation in target tissues. It is interesting that the oft-maligned reporter assays for 3xERE-driven activity and receptor-coactivator interactions showed greater predictive capacity than native gene expression or SRC3 occupancy at *GREB1*, as we recently demonstrated by chromatin-immunoprecipitation assay (Nwachukwu et al., 2016), suggesting that these basic quantitative bioassays provide better estimates of integrated ERα activity.

Significance

Systems approaches such as functional genomics or coregulator profiling have led to seminal contributions to our current understanding of nuclear receptor function. Our work demonstrates that combining these approaches with systems structural biology is enabling us to understand how ligands achieve specific signaling outcomes. We implemented a statistical approach to allow unbiased analyses of multiple crystal structures in parallel, and identified subtle structural perturbations of estrogen receptor alpha (ERα) structure in the sub-0.5 Å range, by different bound synthetic and environmental estrogens. These small perturbations were within the noise of the individual structures but contributed significantly to the diverse endocrine-disrupting activity profiles of environmental estrogens. Incorporating multiple structures into a statistical model enables extraction of the super-resolution structural information that drives allosteric signaling. In addition to predicting endocrine disruption, this approach will also facilitate the rational design of improved therapeutics targeting estrogen receptors and other nuclear receptor family members that constitute one of the major categories of druggable proteins.

Experimental Procedures

Cell Culture

Cell lines (HeLa, HEK293T, HepG2, Ishikawa, MCF-7, MDA-MB231, and U2OS) were obtained from the ATCC and cultured in DMEM (Mediatech) supplemented with 10% fetal bovine serum (FBS) (HyClone, Thermo Scientific), and 1% each of penicillin-streptomycin-neomycin antibiotic mixture, GlutaMAX, and non-essential amino acids (Gibco, Life Technologies), and maintained at a temperature of 37°C in an incubator containing 5% CO_2. Steroid deprivation was achieved by culturing these cells for more than 48 hr in phenol red-free DMEM supplemented with 10% charcoal/dextran-stripped FBS, and 1% each of the antibiotic mixture, GlutaMAX, and non-essential amino acids.

ERα Ligands

Coumestrol (CAS no. 479-13-0), zearalenone (CAS no. 17,924-92-4), and DDT (CAS no. 50-29-3) were purchased from Sigma-Aldrich. The 42 synthetic ligands in the training set (Table S2) have been described previously (Nwachukwu et al., 2016; Srinivasan et al., 2013).

3xERE-Driven Luciferase Assay

Steroid-deprived cells were transfected with 3xERE-luciferase reporter plasmid (MCF-7 and Ishikawa) and human ERα or ERβ expression plasmids (Hela, U2OS, HepG2) using FuGENE HD Reagent (Roche Applied Science). The next day, 10 μM compounds were dispensed. Luciferase activity was measured after 24 hr.

M2H Assay

Steroid-deprived HEK293T cells were transfected in 384-well plates with 10 ng/well of ERα fused to the VP16 activation domain, 20 ng/well of SRC1/2/3 fused to the DBD of yeast Gal4 protein, 10 ng/well of 5xUAS luciferase reporter, and 30 ng/well of pSPORT6 using 0.225 μL/well of LT1 transfection reagent (Mirus Bio). The following day cells were stimulated with 10 μM ligands dispensed using Biomek NXP for 24 hr, after which luciferase activity was measured.

X-Ray Crystallography

Human ERα-Y537S LBD amino acids 298–554 was expressed in *Escherichia coli* and purified as described in Supplemental Experimental Procedures. The LBD solution (1 mM) was mixed with a receptor-interacting peptide of NR coactivator 2 (SRC2) (1.5 mM) and soaking compound 3-methyl-6-phenyl-3H-imidazo[4,5-b]pyridin-2-amine (3–5 mM), incubated overnight at 4°C, and subject to vapor diffusion in hanging-drop format at room temperature. The resulting crystals were soaked with ligands. X-ray diffraction data was collected at the Stanford Synchrotron Radiation Lightsource, beamline 11-1. Diffraction data were reduced using HKL-2000 software (Minor et al., 2006), refined with PHENIX (Adams et al., 2011), and rebuilt with Coot (Emsley et al., 2010). Details are described in Supplemental Experimental Procedures. Images were generated with CCP4mg (McNicholas et al., 2011).

Dimerization

Ligand-dependent formation of ERα homodimers was measured using a previously described bioluminescence resonance energy transfer assay (Powell and Xu, 2008).

DNA Binding

Ligand-dependent binding of ERα-VP16 to a 3xERE-reporter was measured as described previously (Srinivasan et al., 2013), where the strong activation by VP16 overrides the pharmacology of the ER ligand and the signal reflects DNA binding (Pham et al., 1991).

qRT-PCR

Steroid-deprived MCF-7 cells were stimulated with 10 μM ligands for 1 hr (*MYC*) or 24 hr (*GREB1*) in 384-well format using a Biomek NXP workstation (Beckman Coulter). Total RNA was extracted using the RNAGEM Tissue Plus RNA extraction kit (ZyGEM), reverse-transcribed using the Applied Biosystems (ABI) High Capacity cDNA Reverse Transcription Kit (Thermo Fisher Scientific), and analyzed in an ABI 7900HT Real-Time PCR System, using the ABI TaqMan gene expression master mix and assays for *GREB1* (Hs00536412_m1), *MYC* (Hs00153408_m1), and *GADPH* endogenous control (product no. 4333764F) (Thermo Fisher Scientific).

IL-6 ELISA

Steroid-deprived MCF-7 cells in 384-well format were treated with vehicle or 15 ng/mL TNF-α alone or in combination with 10 μM ligands for 24 hr. IL-6 protein levels in the medium were then measured using an IL-6 AlphaLISA kit (PerkinElmer).

Cell Proliferation

MCF-7 and MDA-MB231 cells were plated on 384-well plates in phenol red-free DMEM with 10% FBS and treated 7 hr later with vehicle or 10 μM ligands using a Biomek NXP workstation (Beckman Coulter). After 4 days, treatment was repeated. Three days later, cell viability was determined by measuring luminescence after addition of 20 μL/well CellTitre-Glo reagent (Promega).

Statistical Analysis

Structural and biochemical data were analyzed by linear regression analysis using Prism software (GraphPad Software). To this end, we generated a cross-correlation matrix reporting Pearson's correlation coefficient, r, and p values from the F test for non-zero slope for each pairwise comparison. Multiple (linear) regression analysis with MCF-7 cell proliferation as the dependent variable was performed using StatPlus software (AnalystSoft, version 6).

For error calculations, we obtained estimates of the positional error for the α carbons using the DPI calculated by the DPI server (http://cluster.physics.iisc.ernet.in/dpi/) (Cruickshank, 1999; Kumar et al., 2015). For the averaged distances, the estimated error in the α carbon of an amino acid residue was calculated as $\sigma = \sqrt{\sigma^2_{\text{A chain}} + \sigma^2_{\text{B chain}}}$. The data and calculations are in Data S1.

Hierarchical clustering was used to measure inter-structure dissimilarity for clustering. For each structure, a six-dimension vector $\{\Delta d_{ij}\}$ was constructed with

$$\Delta d_{ij} = d_{ij} - d_{ij}^{E2}, \quad \textbf{(Equation 1)}$$

where d_{ij} is one of the six key distances and the superscript E2 indicates the value from the reference estradiol-bound structure (PDB: 3UUD). Distance between structures was measured with the Euclidean distance of $\{\Delta d_{ij}\}$, which was then employed to do a hierarchical clustering. The number of clusters was determined by visually inspecting the resulting dendrogram from the clustering (Figure 7A). Analyses were performed with Bio3D version 2.0 (Skjaerven et al., 2014). Principal component analysis was employed to characterize the inter-conformer relationship of the 144 crystallographic structures of the estrogen receptor dimer, using Bio3D version 2.0 and as described in detail in Supplemental Experimental Procedures.

Author Contributions

J.C.N. designed and performed the experiments, and wrote the manuscript; S.S., N.B., and J.N. performed the experiments; F.M. and J.A.K. designed and synthesized the compounds; J.C.N., J.N., N.J.W., R.E., T.I., and K.W.N. performed the structural determination; D.J.K., X.Y., and B.J.G. analyzed the structures; O.E. designed the experiments and analyzed the data; J.A.K. and K.W.N. designed the experiments and wrote the manuscript.

Acknowledgments

Research support from the NIH (PHS 5R37DK015556 to J.A.K. and 5R01DK077085 to K.W.N.) is acknowledged. The BallenIsles Men's Golf Association supports J.C.N. The Frenchman's Creek Women for Cancer Research supports S.S. The National Science Foundation (NSF award 1359369) supported N.J.W. Intramural funding support from the University of Pisa (to F.M.) is gratefully acknowledged. University of Michigan start-up funds and the NIH (2R01GM070862-10A1) supports. X.Y. and B.J.G. X-ray diffraction data were collected at the Stanford Synchrotron Radiation Lightsource (SSRL) (beamline 11-1).

Accession Numbers

The structures reported in this paper have been deposited in the PDB and are listed in Data S2.

References

Adams P.D., Afonine P.V., Bunkoczi G., Chen V.B., Echols N., Headd J.J., Hung L.W., Jain S., Kapral G.J., Grosse Kunstleve R.W., et al., The Phenix software for automated determination of macromolecular structures, *Methods* **55**, 2011, 94–106.

Bruning J.B., Parent A.A., Gil G., Zhao M., Nowak J., Pace M.C., Smith C.L., Afonine P.V., Adams P.D., Katzenellenbogen J.A. and Nettles K.W., Coupling of receptor conformation and ligand orientation determine graded activity, *Nat. Chem. Biol.* **6**, 2010, 837–843.

Cruickshank D.W., Remarks about protein structure precision, *Acta Crystallogr. D Biol. Crystallogr.* **55**, 1999, 583–601.

Dasgupta S., Lonard D.M. and O'Malley B.W., Nuclear receptor coactivators: master regulators of human health and disease, *Annu. Rev. Med.* **65**, 2014, 279–292.

Delfosse V., Grimaldi M., Cavailles V., Balaguer P. and Bourguet W., Structural and functional profiling of environmental ligands for estrogen receptors, *Environ. Health Perspect.* **122**, 2014, 1306–1313.

Di Renzo G.C., Conry J.A., Blake J., DeFrancesco M.S., DeNicola N., Martin J.N., Jr., McCue K.A., Richmond D., Shah A., Sutton P., et al., International Federation of Gynecology and Obstetrics opinion on reproductive health impacts of exposure to toxic environmental chemicals, *Int. J. Gynaecol. Obstet.* **131**, 2015, 219–225.

Emsley P., Lohkamp B., Scott W.G. and Cowtan K., Features and development of Coot, *Acta Crystallogr. D Biol. Crystallogr.* **66**, 2010, 486–501.

Ferreira-Dias G., Botelho M., Zagrajczuk A., Rebordao M.R., Galvao A.M., Bravo P.P., Piotrowska-Tomala K., Szostek A.Z., Wiczkowski W., Piskula M., et al., Coumestrol and its metabolite in mares' plasma after ingestion of phytoestrogen-rich plants: potent endocrine disruptors inducing infertility, *Theriogenology* **80**, 2013, 684–692.

Gore A.C., Chappell V.A., Fenton S.E., Flaws J.A., Nadal A., Prins G.S., Toppari J. and Zoeller R.T., Executive Summary EDC-2: the Endocrine Society's second Scientific Statement on endocrine-disrupting chemicals, *Endocr. Rev.* **36**, 2015, E1–E150.

Grese T.A., Sluka J.P., Bryant H.U., Cullinan G.J., Glasebrook A.L., Jones C.D., Matsumoto K., Palkowitz A.D., Sato M., Termine J.D., et al., Molecular determinants of tissue selectivity in estrogen receptor modulators, *Proc. Natl. Acad. Sci. USA* **94**, 1997, 14105–14110.

Kumar V. and Chambon P., The estrogen receptor binds tightly to its responsive element as a ligand-induced homodimer, *Cell* **55**, 1988, 145–156.

Kumar K.S.D., Garusran M., Satheesh S.N., Radha P., Ravithra S., Thulaa Tharshan K.P.S., Helliwell J.R. and Sekar K., Online_DPI: a web server to calculate the diffraction precision index for a protein structure, *J. Appl. Crystallogr.* **48**, 2015, 939–942.

Lonard D.M., Lanz R.B. and O'Malley B.W., Nuclear receptor coregulators and human disease, *Endocr. Rev.* **28**, 2007, 575–587.

McInerney E.M. and Katzenellenbogen B.S., Different regions in activation function-1 of the human estrogen receptor required for antiestrogen- and estradiol-dependent transcription activation, *J. Biol. Chem.* **271**, 1996, 24172–24178.

McInerney E.M., Weis K.E., Sun J., Mosselman S. and Katzenellenbogen B.S., Transcription activation by the human estrogen receptor subtype beta (ER beta) studied with ER beta and ER alpha receptor chimeras, *Endocrinology* **139**, 1998, 4513–4522.

McNicholas S., Potterton E., Wilson K.S. and Noble M.E., Presenting your structures: the CCP4mg molecular-graphics software, *Acta Crystallogr. D Biol. Crystallogr.* **67**, 2011, 386–394.

Metivier R., Penot G., Hubner M.R., Reid G., Brand H., Kos M. and Gannon F., Estrogen receptor-alpha directs ordered, cyclical, and combinatorial recruitment of cofactors on a natural target promoter, *Cell* **115**, 2003, 751–763.

Minor W., Cymborowski M., Otwinowski Z. and Chruszcz M., HKL-3000: the integration of data reduction and structure solution – from diffraction images to an initial model in minutes, *Acta Crystallogr. D Biol. Crystallogr.* **62**, 2006, 859–866.

Montano M.M., Muller V., Trobaugh A. and Katzenellenbogen B.S., The carboxy-terminal F domain of the human estrogen receptor: role in the transcriptional activity of the receptor and the effectiveness of antiestrogens as estrogen antagonists, *Mol. Endocrinol.* **9**, 1995, 814–825.

Nettles K.W., Bruning J.B., Gil G., Nowak J., Sharma S.K., Hahm J.B., Kulp K., Hochberg R.B., Zhou H., Katzenellenbogen J.A., et al., NFkappaB selectivity of estrogen receptor ligands revealed by comparative crystallographic analyses, *Nat. Chem. Biol.* **4**, 2008, 241–247.

Nwachukwu J.C., Southern M.R., Kiefer J.R., Afonine P.V., Adams P.D., Terwilliger T.C. and Nettles K.W., Improved crystallographic structures using extensive combinatorial refinement, *Structure* **21**, 2013, 1923–1930.

Nwachukwu J.C., Srinivasan S., Bruno N.E., Parent A.A., Hughes T.S., Pollock J.A., Gjyshi O., Cavett V., Nowak J., Garcia-Ordonez R.D., et al., Resveratrol modulates the inflammatory response via an estrogen receptor-signal integration network, *Elife* **3**, 2014, e02057.

Nwachukwu J.C., Srinivasan S., Zheng Y., Wang S., Min J., Dong C., Liao Z., Nowak J., Wright N.J., Houtman R., et al., Predictive features of ligand-specific signaling through the estrogen receptor, *Mol. Syst. Biol.* **12**, 2016, 864.

Patel S.R. and Skafar D.F., Modulation of nuclear receptor activity by the F domain, *Mol. Cell. Endocrinol.* **418**, 2015, 298–305.

Pham T.A., Elliston J.F., Nawaz Z., McDonnell D.P., Tsai M.J. and O'Malley B.W., Antiestrogen can establish nonproductive receptor complexes and alter chromatin structure at target enhancers, *Proc. Natl. Acad. Sci. USA* **88**, 1991, 3125–3129.

Powell E. and Xu W., Intermolecular interactions identify ligand-selective activity of estrogen receptor alpha/beta dimers, *Proc. Natl. Acad. Sci. USA* **105**, 2008, 19012–19017.

Rokavec M., Wu W. and Luo J.L., IL6-mediated suppression of miR-200c directs constitutive activation of inflammatory signaling circuit driving transformation and tumorigenesis, *Mol. Cell* **45**, 2012, 777–789.

Schoevers E.J., Santos R.R., Colenbrander B., Fink-Gremmels J. and Roelen B.A., Transgenerational toxicity of Zearalenone in pigs, *Reprod. Toxicol.* **34**, 2012, 110–119.

Schwabe J.W., Chapman L., Finch J.T. and Rhodes D., The crystal structure of the estrogen receptor DNA-binding domain bound to DNA: how receptors discriminate between their response elements, *Cell* **75**, 1993, 567–578.

Shang Y. and Brown M., Molecular determinants for the tissue specificity of SERMs, *Science* **295**, 2002, 2465–2468.

Skjaerven L., Yao X.Q., Scarabelli G. and Grant B.J., Integrating protein structural dynamics and evolutionary analysis with Bio3D, *BMC Bioinformatics* **15**, 2014, 399.

Srinivasan S., Nwachukwu J.C., Parent A.A., Cavett V., Nowak J., Hughes T.S., Kojetin D.J., Katzenellenbogen J.A. and Nettles K.W., Ligand-binding dynamics rewire cellular signaling via estrogen receptor-alpha, *Nat. Chem. Biol.* **9**, 2013, 326–332.

Thompson M.A., Lew M.D. and Moerner W.E., Extending microscopic resolution with single-molecule imaging and active control, *Annu. Rev. Biophys.* **41**, 2012, 321–342.

E-Extra

Keywords: nuclear receptor; steroid hormone; endocrine disruptor; estrogen receptor-α; breast cancer; X-ray crystallography; allosteric signaling

Graphical Abstract

ELSEVIER_CCBIO_200